Depletion-electric-field-induced second-harmonic generation near oxidized GaAs(001) surfaces

Thomas A. Germer, Kurt W. Kołasiński,* John C. Stephenson, and Lee J. Richter†
National Institute of Standards and Technology, Gaithersburg, Maryland 20899
(Received 23 September 1996; revised manuscript received 12 December 1996)

Second-order nonlinear mixing is evaluated as a probe of the depletion electric field in the near-surface region of GaAs(001). A phenomenological model is presented whereby the nonlinear susceptibility is expanded in the depletion electric field. For GaAs, three terms contribute to the observed nonlinear mixing: the dipole-allowed bulk contribution and first- and second-order contributions in the depletion electric field. All three contributions can be isolated by a combination of rotational anisotropy and photomodulation studies. The second-harmonic signal from oxidized GaAs(001) surfaces was measured as a function of azimuthal sample orientation, photomodulation, and dopant density for fundamental photon energies in the region 1.17–1.51 eV. The first-order depletion-electric-field contribution dominates the second-order contribution, and can be comparable to the intrinsic bulk contribution for high surface fields. The results rule out significant contributions arising from either bulk electric quadrupole or surface dipole effects. [S0163-1829(97)00616-4]

I. INTRODUCTION

Second-harmonic generation (SHG) has been identified as a tool for studying interfaces due to its inherent surface sensitivity in centrosymmetric materials.[1,2] This sensitivity results from symmetry constraints on the bulk second-order susceptibility $\chi^{(2)}$, which is zero in the dipole approximation when the material contains a center of inversion. However, higher-order bulk terms may contribute to SHG, including those arising from electric quadrupole[3] and higher-order electric dipole responses. These other terms ultimately limit the surface sensitivity of the technique; therefore, a thorough analysis must be carried out before results can be interpreted as arising from a surface susceptibility.

GaAs is not centrosymmetric, and a significant signal arises from the bulk dipole susceptibility. A surface-induced signal, however, can be effectively separated from the bulk-induced signal by an appropriate choice of the experimental geometry.[4,5] Numerous researchers have addressed SHG from GaAs, and have interpreted their results in light of a surface nonlinear susceptibility.[4,6–11] Several recent reports have demonstrated convincingly that depletion-electric-field-induced second-harmonic generation (depletion-EFISH) can dominate surface contributions in a number of semiconducting samples.[12–16] In the present paper, we demonstrate the importance of the depletion electric field in modifying the SHG observed from oxidized GaAs(001), and conclude that nearly all of the signal attributed to the reduction of symmetry at the surface of highly doped samples results from the near-surface depletion electric field.

In Sec. II, a phenomenological model of EFISH is presented. This model concludes that EFISH contributes to the second-harmonic rotational anisotropy in first order isotropically and in second order anisotropically, the latter interfering directly with the unperturbed bulk-generated field. In Sec. III, details of the experimental methods used in this study are given. In Sec. IV, the results of those experiments are presented. The results are further discussed in Sec. V. Analysis of the SHG as a function of both sample doping and optical pumping convincingly demonstrates that surface SHG can be ignored in these studies and that a large part of the total signal is due to a first-order contribution from the depletion electric field.

II. MODEL

A depletion electric field near a GaAs(001) surface lowers the symmetry of the GaAs bulk from $43m$ to $mm2$. In this section, we will describe how this lowering of symmetry affects the nonlinear susceptibility and thus the second-harmonic signal from GaAs(001) in the presence of a depletion electric field.

A. Effective second-order susceptibility in the presence of a field

Throughout this paper we will use the coordinate system natural to $43m$ where, by convention, the Ga-As bonds point in the [111], [1$\bar{1}$1], [11$\bar{1}$], and [1$\bar{1}\bar{1}$] directions. The outward surface normal is defined to be $\hat{\mathbf{z}}$, and $\hat{\mathbf{x}}$ and $\hat{\mathbf{y}}$ lie in the surface plane, at 45° to the surface nearest-neighbor directions. Note that the basis vectors $\hat{\mathbf{x}}$ and $\hat{\mathbf{y}}$ of this coordinate system are not those usually associated with representation of the $mm2$ group.[8,17]

We assume that χ^{eff} in the dipole approximation can be expanded in terms of the applied field,

$$\begin{aligned}\chi_{ijk}^{(\mathrm{eff})} = {} & \chi_{ijk}^{(2)}(-\omega_1-\omega_2;\omega_1,\omega_2) \\ & + 3\chi_{ijkz}^{(3)}(-\omega_1-\omega_2;\omega_1,\omega_2,0)E_z^{(\mathrm{depl})} \\ & + 6\chi_{ijkzz}^{(4)}(-\omega_1-\omega_2;\omega_1,\omega_2,0,0)E_z^{(\mathrm{depl})2} \\ & + O(E_z^{(\mathrm{depl})3}),\end{aligned} \tag{1}$$

where $\chi^{(2)}$, $\chi^{(3)}$, and $\chi^{(4)}$ have symmetry properties of the $43m$ bulk crystal. The factors of 3 and 6 account for permutations of the zero-frequency indices. There are six nonvanishing elements of $\chi^{(2)}$ in $43m$ symmetry; all are equivalent by symmetry and have indices

$$xyz = yzx = zxy = xzy = zyx = yxz. \tag{2}$$

There are 22 nonzero elements of $\chi^{(3)}$, four of which are unique: $iijj$, $ijij$, $ijji$, and $iiii$ $(i\neq j)$. When contracted with the electric field $E_z^{(\mathrm{depl})}$, these elements give rise to four unique nonzero elements of $\chi^{(3)}_{ijkz}E_z^{(\mathrm{depl})}$:

$$zzz, xxz=yyz,\ xzx=yzy \quad \text{and} \quad zxx=zyy. \tag{3}$$

Similarly, there are 60 nonzero elements of $\chi^{(4)}$, ten of which are unique: $iiijk$, $iijik$, $iijki$, $ijiik$, $ijiki$, $ijkii$, $jiiik$, $jiiki$, $jikii$, and $jkiii$ $(i\neq j\neq k)$. Three independent elements of $\chi^{(4)}_{ijkzz}E_z^{(\mathrm{depl})2}$ arise from these:

$$xyz=yxz, \quad xzy=yzx, \quad \text{and} \quad zxy=zyx. \tag{4}$$

It can be easily shown that, at second order in $E_z^{(\mathrm{depl})}$, the seven unique nonzero elements of $\chi^{(\mathrm{eff})}$ are those expected for $mm2$ symmetry. For second-harmonic generation, where $\omega_1=\omega_2$ (and the second and third indices are interchangeable), the effective susceptibility elements are

$$\chi^{(\mathrm{eff})}_{xxz}=\chi^{(\mathrm{eff})}_{yyz}=\chi^{(\mathrm{eff})}_{xzx}=\chi^{(\mathrm{eff})}_{yzy}=3\chi^{(3)}_{xxzz}E_z^{\mathrm{depl}},$$

$$\chi^{(\mathrm{eff})}_{zxx}=\chi^{(\mathrm{eff})}_{zyy}=3\chi^{(3)}_{zxxz}E_z^{(\mathrm{depl})},$$

$$\chi^{(\mathrm{eff})}_{zzz}=3\chi^{(3)}_{zzzz}E_z^{(\mathrm{depl})}, \tag{5}$$

$$\chi^{(\mathrm{eff})}_{xzy}=\chi^{(\mathrm{eff})}_{yzx}=\chi^{(\mathrm{eff})}_{yxz}=\chi^{(\mathrm{eff})}_{xyz}=\chi^{(2)}_{xyz}+6\chi^{(4)}_{xyzzz}E_z^{(\mathrm{depl})^2},$$

$$\chi^{(\mathrm{eff})}_{zxy}=\chi^{(\mathrm{eff})}_{zyx}=\chi^{(2)}_{xyz}+6\chi^{(4)}_{zxyzz}E_z^{(\mathrm{depl})^2}.$$

B. Second-harmonic signal resulting from the nonlinear polarization

We will consider only a linearly polarized incident electric field given by

$$\mathbf{E}(\mathbf{r},t)=(E_s\hat{\mathbf{s}}+E_p\hat{\mathbf{p}})e^{i(\mathbf{k}\cdot\mathbf{r}-\omega t)}+\text{c.c.}, \tag{6}$$

where $\hat{\mathbf{s}}$ is a unit vector given by $\hat{\mathbf{s}}=\hat{\mathbf{k}}\times\hat{\mathbf{z}}$, and $\hat{\mathbf{p}}$ is a unit vector given by $\hat{\mathbf{s}}\times\hat{\mathbf{k}}$. The second-order polarization inside the material is then given (in the mks system) by

$$P_i^{(\mathrm{dipole})}(2\omega)=\varepsilon_0\chi^{(\mathrm{eff})}_{ijk}(-2\omega;\omega,\omega)E_j^{(\mathrm{inside})}E_k^{(\mathrm{inside})}, \tag{7}$$

where ε_0 is the permittivity of free space, and $E^{(\mathrm{inside})}$ is the Fourier transform of the field given by Eq. (6), measured inside the material. This polarization will give rise to a radiated electric field with frequency 2ω.

The total field radiated by this nonlinear polarization will depend on the orientation of the crystal, the polarization state of the incoming radiation, the angle of incidence, and the dielectric properties of the crystal. The derivation of the radiated field follows the discussions of Refs. 18 and 19. For linearly polarized input fields incident on a GaAs(001) surface, it can be shown that the radiated second harmonic fields $E^{(\mathrm{dipole})}_{\mathrm{out\ in}}$ resulting from $\chi^{(\mathrm{eff})}$ are given in terms of the input electric fields E_p, E_s, and $E_{\bar{q}}[\bar{q}\equiv(\hat{\mathbf{p}}-\hat{\mathbf{s}})/\sqrt{2}]$ measured *outside* the material by

$$E_{pp}^{(\mathrm{dipole})}=E_p^2t_p^2\{B_p^{(3)}(-f_s^2F_s\chi^{(3)}_{zzzz}+2f_cf_sF_c\chi^{(3)}_{xxzz}-f_c^2F_s\chi^{(3)}_{zxxz})+[B_p^{(2)}(2f_cf_sF_c-f_c^2F_s)\chi^{(2)}_{xyz}-B_p^{(4)}\times(f_c^2F_s\chi^{(4)}_{zxyzz}-2f_cf_sF_c\chi^{(4)}_{xzyzz})]\sin 2\phi\}, \tag{8}$$

$$E_{sp}^{(\mathrm{dipole})}=2E_p^2f_cf_st_p^2(B_s^{(2)}\chi^{(2)}_{xyz}+B_s^{(4)}\chi^{(4)}_{xyzzz})\cos2\phi, \tag{9}$$

$$E_{ps}^{(\mathrm{dipole})}=-E_s^2F_st_s^2[B_p^{(3)}\chi^{(3)}_{zxxz}-(B_p^{(2)}\chi^{(2)}_{xyz}+B_p^{(4)}\chi^{(4)}_{zxyzz})\sin2\phi], \tag{10}$$

$$E_{p\bar{q}}^{(\mathrm{dipole})}=\frac{E_{\bar{q}}^2}{2}(B_p^{(2)}\chi^{(2)}_{xyz}\{[(2f_cf_sF_c-f_c^2F_s)t_p^2+F_st_s^2]\sin2\phi+(-2f_sF_c+2f_cF_s)t_st_p\cos2\phi\}+B_p^{(3)}\times[(-f_c^2F_s\chi^{(3)}_{zxxz}+2f_sf_cF_c\chi^{(3)}_{xxzz}-f_s^2F_s\chi^{(3)}_{zzzz})t_p^2-F_s\chi^{(3)}_{zxxz}t_s^2]+B_p^{(4)}\{[(2f_sf_cF_c\chi^{(4)}_{xyzzz}-f_c^2F_s\chi^{(4)}_{zxyzz})t_p^2+F_s\chi^{(4)}_{zxyzz}t_s^2]\sin2\phi-(2f_cF_s\chi^{(4)}_{zxyzz}-2f_sF_c\chi^{(4)}_{xyzzz})t_st_p\cos2\phi\}), \tag{11}$$

$$E_{s\bar{q}}^{(\mathrm{dipole})}=E_{\bar{q}}^2[B_s^{(2)}\chi^{(2)}_{xyz}(f_sf_ct_p^2\cos2\phi-f_st_st_p\sin2\phi)+B_s^{(3)}\chi^{(3)}_{xxzz}f_st_st_p+B_s^{(4)}\chi^{(4)}_{xyzzz}(f_sf_ct_p^2\cos2\phi-f_st_st_p\sin2\phi)], \tag{12}$$

and

$$E_{ss}^{(\mathrm{dipole})}=0, \tag{13}$$

where ϕ is the rotation of the [100] direction out of the plane of incidence, $B^{(2)}_{p,s}$ $[=-B_{p,s}/(4\pi)$ in the notation of Ref. 18] is given by

$$B^{(2)}_{p,s}=-\frac{i\Omega^2T_{p,s}}{2W}\int_{-\infty}^{0}e^{-ipz}dz=\frac{\Omega^2T_{p,s}}{2pW}, \tag{14}$$

and the phase parameter $p=2w+W$. The terms for $B^{(3)}_{p,s}$ and $B^{(4)}_{p,s}$ can be similarly derived to be

$$B^{(3)}_{p,s}=-\frac{3i\Omega^2T_{p,s}}{2W}\int_{-\infty}^{0}E_z^{(\mathrm{depl})}(z)e^{-ipz}dz \tag{15}$$

and

$$B^{(4)}_{p,s}=-\frac{3i\Omega^2T_{p,s}}{W}\int_{-\infty}^{0}E_z^{(\mathrm{depl})2}(z)e^{-ipz}dz. \tag{16}$$

The terms f_c, f_s, F_c, and F_s are the complex cosine and sine of the fundamental and second-harmonic internal angles; $\Omega=2\omega/c$, w and W are the components of the wave vectors of the fundamental and second-harmonic light in the direction perpendicular to the surface; and $t_s(t_p)$ and $T_s(T_p)$ are the transmission coefficients of the fundamental light into and the second-harmonic light out of the crystal for s- (p-) polarized light. Explicit expressions for these parameters are given in the Appendix.

If the surface potential with respect to the bulk Fermi level is Φ_0, and the Debye screening length is L_D, then, to a good approximation,[20]

$$E^{(\mathrm{depl})}(z)=\frac{2\Phi_0(z+L_D)}{L_D^2} \tag{17}$$

for $0>z>-L_D$ and $E^{(\mathrm{depl})}(z)=0$ elsewhere. Inserting Eq. (17) into Eqs. (15) and (16), and integrating, one obtains

$$B_{p,s}^{(3)}=-\frac{3i\Omega^2 T_{p,s}\Phi_0}{L_D^2 p^2 W}(1-e^{iL_D p}+iL_D p) \tag{18}$$

and

$$B_{p,s}^{(4)}=-\frac{12i\Omega^2 T_{p,s}\Phi_0^2}{L_D^4 p^3 W}(2ie^{iL_D p}-2i+2L_D p+iL_D^2 p^2). \tag{19}$$

The total radiated field may also include contributions that are quadrupolar in the incoming field,

$$P_i^{(\mathrm{quad})}=\varepsilon_0\Gamma_{ijkl}E_j^{(\mathrm{inside})}\nabla_k E_l^{(\mathrm{inside})}, \tag{20}$$

where Γ is the quadrupolar nonlinear susceptibility, and, from a surface nonlinear susceptibility $\Delta^{(2)}$,

$$P_i^{(\mathrm{surf})}=\varepsilon_0\Delta_{ijk}^{(2)}E_j^{(\mathrm{inside})}E_k^{(\mathrm{inside})}\delta(z-z_0^+), \tag{21}$$

which has typically been considered to be outside the surface, even though the fields are evaluated inside the surface.[21] The fields radiated by these polarizations were derived in detail by Sipe, Moss, and van Driel.[18]

In the case of SHG from a single plane wave, the field radiated by the quadrupolar nonlinear polarization can be quantified by two parameters: $\gamma=\Gamma_{xyxy}/2$ and $\zeta=\Gamma_{xxxx}-\Gamma_{xyyx}-\Gamma_{xyxy}-\Gamma_{xxyy}$, the isotropic and anisotropic terms, respectively. For an isotropic material $\zeta=0$ but can be nonzero for $43m$ symmetry, while γ is nonzero even for an isotropic medium.

The bulk-terminated GaAs(001) surface has $mm2$ symmetry, which is the same as that of the near-surface bulk in the presence of the depletion electric field; therefore, rotational anisotropy studies cannot distinguish signal from a $mm2$ surface from the depletion-electric-field-induced signal. A disordered oxide surface has a macroscopic ∞ symmetry, and will not produce an anisotropic response.

The total detected field is the sum of the various contributions. In our experiments, the nonlinear signal from the sample is normalized to the nonlinear response of a reference. The observed signal ratio can be parametrized by

$$S_{ij}(\phi)\propto\frac{|E_{ij}(2\omega,\phi)|^2}{|E_j(\omega)|^4}=\left|a_{ij}+\sum_{m=1}^{4}[b_{ij}^{(m)}\sin m\phi+c_{ij}^{(m)}\cos m\phi]\right|^2, \tag{22}$$

where the proportionality depends on the geometry and $\chi^{(2)}$ of the reference material. For the $43m$ and $mm2$ symmetries considered here, only even m terms contribute to the sum. Table I reviews which tensor elements contribute to the field parameters a, b, and c. Notice that the depletion electric field contributes in first order to a only and in second order to $b^{(2)}$ and $c^{(2)}$ only. In Ref. 16, it is incorrectly stated that the depletion electric field contributes linearly to $b^{(2)}$ and $c^{(2)}$. Also, note that the ζ contribution can be uniquely determined from the $b^{(4)}$ and $c^{(4)}$ terms.

TABLE I. The field parameters [see Eq. (22)] arising from the different susceptibility tensors. $\chi^{(2)}$ is the bulk dipole allowed tensor; $\chi^{(3)}$ and $\chi^{(4)}$ are the EFISH expansion tensors; $\Delta^{(2)}$ is the pure surface tensor; γ and ζ are bulk quadrupolar terms. − indicates no contribution.

	pp (out, in)	$p\overline{q}$	ps	sp	$s\overline{q}$	ss
$\chi^{(2)}_{xyz}$	$b^{(2)}$	$b^{(2)},c^{(2)}$	$b^{(2)}$	$c^{(2)}$	$c^{(2)},b^{(2)}$	−
$\chi^{(3)}_{zzzz}$, Δ_{zzz}	a	a	−	−	−	−
$\chi^{(3)}_{zxxz}$, Δ_{zxx}	a	a	a	−	−	−
$\chi^{(3)}_{xxzz}$, Δ_{xxz}	a	a	−	−	a	−
$\chi^{(4)}_{xyzzz}$, Δ_{xyz}	$b^{(2)}$	$b^{(2)},c^{(2)}$	−	$c^{(2)}$	$c^{(2)},b^{(2)}$	−
$\chi^{(4)}_{zxyzz}$, Δ_{zxy}	$b^{(2)}$	$b^{(2)},c^{(2)}$	$b^{(2)}$	−	−	−
γ	a	a	a	−	−	−
ζ	$a,c^{(4)}$	$a,c^{(4)},b^{(4)}$	$a,c^{(4)}$	$b^{(4)}$	$a,b^{(4)},c^{(4)}$	$b^{(4)}$

III. EXPERIMENT

Figure 1 is a schematic overview of the second-harmonic experiment. Tunable and polarized probe light pulses were focused onto GaAs(001) samples in air at an incident angle of 45° with respect to the surface normal. Second-harmonic light radiating in the specular direction was then collected, filtered, and detected. The samples could be rotated about their surface normal. In the range of 1.32–1.51 eV, probe fundamental light was produced by a dye laser synchronously pumped by the second harmonic of a fiber-compressed mode-locked Nd:YAG (yttrium aluminum garnet) laser. Two dyes were used to span the range. The output of the dye laser was amplified in two stages pumped with the second harmonic of a Nd:YAG regenerative amplifier, operating at a repetition rate of 1 kHz. The nominal duration of the amplified dye-laser-pulses was ≈700 fs full width at half maximum (FWHM). Probe fundamental light at 1.17 eV was obtained from the residual fundamental of the regenerative Nd:YAG amplifier. The Gaussian beam diameter $2w_0$ (full

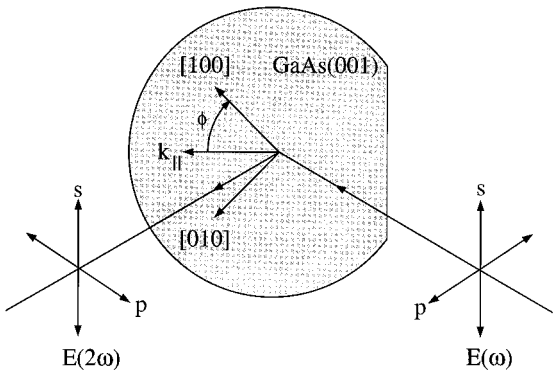

FIG. 1. Schematic representation of the experiment. Linearly polarized light at frequency ω is incident on the sample at 45°. The sample is rotated azimuthally such that the [100] direction is at an angle ϕ with respect to the plane of incidence.

width at $1/e^2$ intensity) of the probe was $\approx$0.22 mm at the sample.

A combination of colored glass filters and a monochromator was used to filter the second-harmonic light, which was polarization analyzed with a Glan-Taylor polarizer and detected with a photomultiplier tube. To allow for shot-to-shot normalization and wavelength-to-wavelength spectral normalization, a small amount of the fundamental light was separated before the GaAs samples, and focused at a conjugate position on a phase-matched, 1-mm-thick β-barium-borate (BBO) crystal. The second-harmonic light generated in the reference arm passed through matched filters and the same monochromator before striking a second photomultiplier tube.

It was found that the probe fundamental can generate sufficient carriers to photomodulate the signal. In order to avoid probe-induced photomodulation of the second-harmonic signal, the probe light was attenuated so that, at most, about 25% of the laser shots yielded detected second-harmonic photons. The output of the photomultiplier tube was gate integrated, and compared to a setpoint, yielding a binary signal β. The reference-normalized signal β/r was also recorded, where r is the reference arm analog signal from a second gated integrator. The average number of recorded counts $\langle\beta\rangle$ and its standard deviation σ_β were adjusted to account for multiple photons striking the detectors by making the transformations[22]

$$\langle\beta\rangle' \leftarrow -\ln(1-\langle\beta\rangle) \tag{23}$$

and

$$\sigma'_\beta \leftarrow \frac{\sigma_\beta}{1-\langle\beta\rangle}. \tag{24}$$

The averaged normalized signal $\langle\beta/r\rangle$ and its standard deviation $\sigma_{\beta/r}$ were likewise scaled,

$$\left\langle\frac{\beta}{r}\right\rangle' \leftarrow -\left\langle\frac{\beta}{r}\right\rangle \frac{\ln(1-\langle\beta\rangle)}{\langle\beta\rangle} \tag{25}$$

and

$$\sigma'_{\beta/r} \leftarrow \frac{\sigma_{\beta/r}}{1-\langle\beta\rangle}. \tag{26}$$

All error bars shown with data are the standard deviation of the mean, $\sigma'_{\beta/r}/\sqrt{N}$. Data were then fit in a weighted least squares sense to Eq. (22) to yield an isotropic field parameter $|a|$, anisotropic field parameters $|b^{(m)}|$ and $|c^{(m)}|$, and the magnitude of their relative phases $|\delta\phi_{ab(m)}|$ and $|\delta\phi_{ac(m)}|$. In the fitting procedure, a small offset in the azimuthal angle ϕ was also adjusted, to account for misalignment of the samples on the rotational stage. All reported uncertainties in the fit parameters are one standard deviation, derived from the elements of the inverse of the curvature matrix.[23]

Over the wavelength range studied, the calculated type-I critical phase-matching angle in BBO (Refs. 24 and 25) varies from 22.77° to 28.46°. This change in phase-matching angle gives a calculated 5% change in nonlinear coefficient $d_{\rm eff}$. The Miller's rule estimate of the dispersion of d_{22} for BBO over the same range gives a 3% effect. These small, monotonic corrections have not been applied to the presented data.

Photons at 2.33 eV were generated by doubling residual 1.17-eV light from the regenerative amplifier and used as a photomodulation source (pump). The 2.33-eV pulses were approximately 180-ps FWHM with a diameter $2w_0$ of 2 mm and a typical pulse energy of 19 μJ. This light was directed onto the sample at a 30° angle of incidence, about 600 ps before the probe. Studies using shorter pump pulses (600 fs), at a wavelength of 635 nm, probed by SHG of 1575 nm generated by difference frequency mixing the residual 1.17-eV light from the regenerative amplifier with the pump, demonstrated that the modulation of the SHG occurred within the cross-correlation of the two pulses (850 fs) and relaxed on a 2–3-ns time scale.

All of the samples, with the exception of one, were polished horizontal-gradient-freeze-grown crystals. The n-type dopant was Si, and the p-type dopant Zn. The 5×10^{16}-cm^{-3} doped sample was a 2-μm-thick layer, molecular beam epitaxy grown on semi-insulating material. All results presented were obtained after the samples were treated with a P_2S_5 surface passivation etch.[26] This etch results in a thin stable oxide. No significant difference could be observed between preliminary results obtained with the as-received n-type samples and the results from the passivated n-type samples. The absolute orientations of the samples were determined by etching sections of the same wafers in 1:8:8 H_2SO_4:H_2O_2:H_2O which preferentially etches in the [110] direction.[27]

IV. RESULTS

Figure 2 shows the second-harmonic signal ratios $S_{\rm pp}(\phi)$, $S_{sp}(\phi)$, and $S_{ps}(\phi)$, for a 3.8×10^{18}-cm^{-3} n-type GaAs(001) sample irradiated at 1.38 eV. The curves drawn through the data represent best fits to Eq. (22). The agreement between the data and the curves is excellent; any deviation from the curves which systematically breaks the $mm2$ symmetry of the data is probably a result of a small miscut of the crystal orientation.[28]

The signal $S_{ss}(\phi)$ was below our detection sensitivity, and is not included in Fig. 2. Since $S_{ss}(\phi)$ only receives a contribution from the quadrupolar term ζ, and since no $\sin4\phi$ term was ever needed to fit the $S_{pp}(\phi)$ or $S_{ps}(\phi)$ data, we obtain an upper limit of $|\zeta|<0.4|\chi^{(2)}_{xyz}|/\Omega$.

The $mm2$ symmetry of the p-out data indicates that isotropic contributions to the signal are significant. The analysis of Sec. II demonstrated that an isotropic contribution can arise from a true surface dipole response via $\Delta^{(2)}$, from the depletion electric field via $\chi^{(3)}$, and from the isotropic quadrupolar term γ. The contribution of γ to SHG cannot be practically resolved from that due to $\Delta^{(2)}_{zxx}$ by rotational anisotropy studies.[29] As ζ is negligible, and γ is of comparable magnitude to ζ in other cubic materials,[30] we will neglect both quadrupolar terms. Additionally, to simplify the notation, we will suppress the (2) on the nonzero anisotropic parameters b and c. To assess the relative contributions of $\Delta^{(2)}$ and $\chi^{(3)}$ to the isotropic response, $S_{pp}(\phi)$ was measured for a series of differently doped, n-type samples. Figure 3 shows the fit parameters $|a_{pp}|$, $|b_{pp}|$, and $|\delta\phi_{ab}|$ as functions

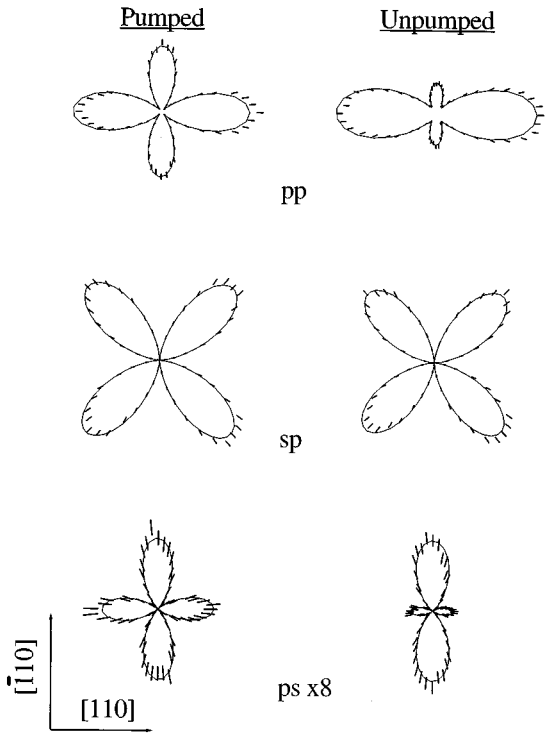

FIG. 2. SH signal as a function of azimuthal orientation for a 3.8×10^{18}-cm^{-3} n-type GaAs(001) sample at $\lambda_1=900$ nm for different detection and input polarizations, with and without 532-nm pumping. The notation sp indicates s-polarized detection and p-polarized input. The arrows mark when $k_{\|}$ is along the indicated crystal axis. The solid lines are fits to Eq. (22). The length of the data lines demarks ± one standard deviation of the mean.

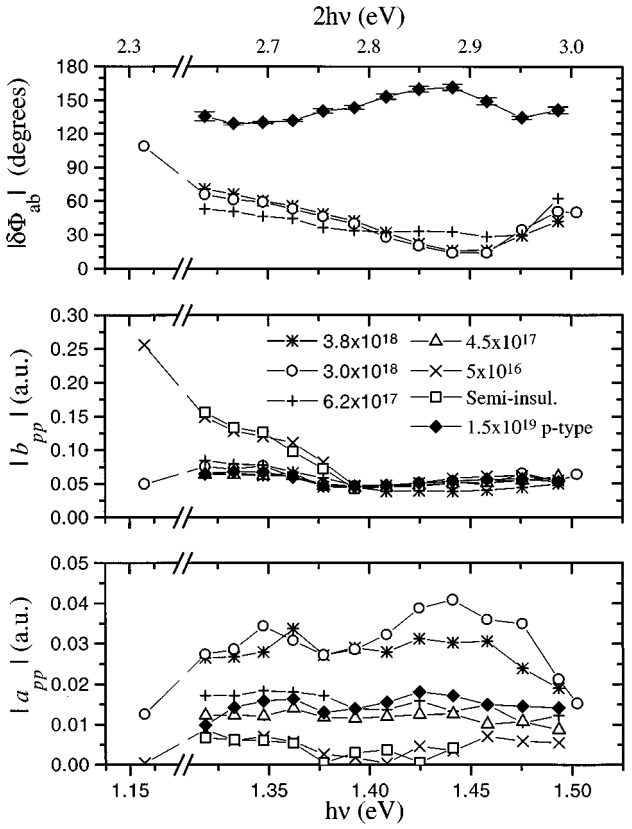

FIG. 3. The field parameters $|a_{pp}|$, $|b_{pp}|$, and $|\delta_{ab}|$ as functions of wavelength for a variety of samples. All samples were n type, unless specified. Typical estimated errors are displayed for $|\delta_{ab}|$ of the p-type sample. The estimated errors in $|a_{pp}|$ and $|b_{pp}|$ are less than the symbol size.

of wavelength for the series. The isotropic field parameter $|a_{pp}|$ tends to increase with dopant concentration over the n-type samples, and exhibits relatively weak dispersion over the studied probe photon energy range. In contrast, the anisotropic parameter $|b_{pp}|$ is relatively independent of both dopant concentration and probe photon energy over the range 1.4–1.5 eV. However, $|b_{pp}|$ exhibits very strong dispersion below 1.4 eV for the 5×10^{16}-cm^{-3} n-type sample and the semi-insulating sample. There is a distinct minimum in $|\delta\phi_{ab}|$ near 1.45 eV for the highly doped n-type samples. Sum-frequency generation (SFG) experiments ($\omega_1+\omega_2=\omega_3$; $\omega_1\neq\omega_2$) were performed with $\hbar\omega_2=1.165$ eV (residual light from the regenerative amplifier) and ω_1 from the tunable dye laser. The minimum in $|\delta\phi_{ab}|$ was not observed for $\hbar\omega_1\approx1.4$ eV, suggesting it is a 2ω feature in the SHG measurements. The monotonic increase in $|b_{pp}|$ was observed for the semi-insulating and 5×10^{16} cm^{-3} samples for both SHG and SFG at fundamental photon energies below 1.40 eV, indicating that it is an ω_1 feature.

To illustrate the distinct sample dependence of the a and b parameters, Fig. 4 shows $|a_{pp}|$ and $|b_{pp}|$ as functions of depletion electric field at the surface, averaged over the fundamental region 1.39–1.51 eV. This wavelength region was chosen since it avoids the region below 1.38 eV where the lightly doped samples show an anomalously large $|b_{pp}|$. The electric fields have been obtained from Eq. (17) and calculated depletion lengths,

$$L_D=\sqrt{2\varepsilon_r\varepsilon_0\Phi_0/qN}, \tag{27}$$

where ε_r is the relative dielectric constant, N is the dopant density, q is the charge of the electron and the surface barrier Φ_0 is 0.68 eV.[31] The parameter $|b_{pp}|$ shows relatively little

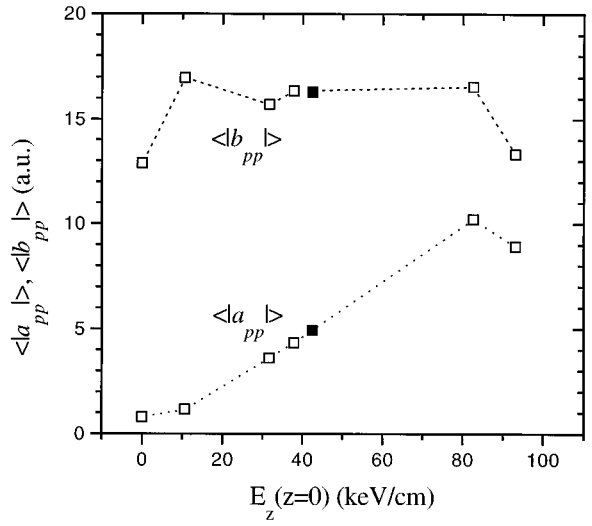

FIG. 4. The spectral average (1.39–1.51 eV) of $|a_{pp}|$ and $|b_{pp}|$ as functions of depletion electric field. The open symbols are n-type samples, the solid symbol is for the 1.5×10^{19}-cm^{-3} p-type sample.

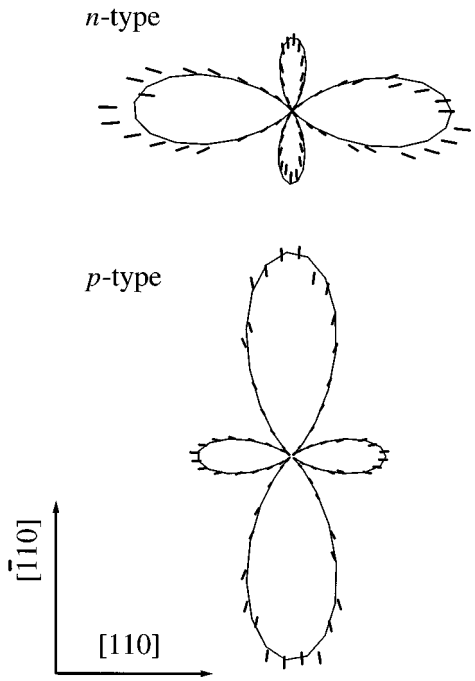

FIG. 5. Radial plot of the second-harmonic signal $S_{pp}(\phi)$ for a fundamental photon energy of 1.46 eV from (a) a 3.0×10^{18}-cm^{-3}, Si-doped n-type sample, and (b) a 1.5×10^{19}-cm^{-3} Zn-doped p-type sample. Note the change in the orientation of the location of the maxima.

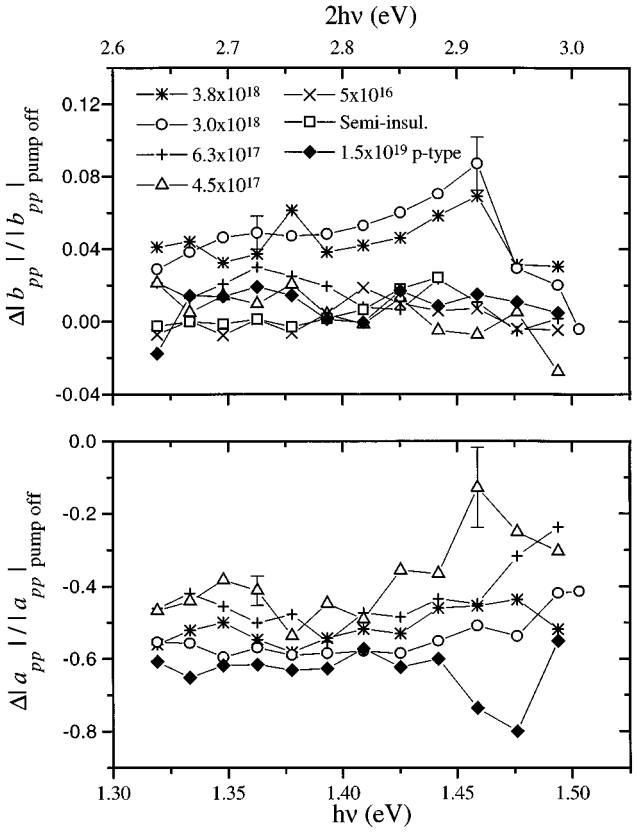

FIG. 6. The 532-nm pump induced changes in the field parameters $|a_{pp}|$ and $|b_{pp}|$ as functions of wavelength for a variety of different samples. $\Delta a \equiv (a_{\text{pump on}} - a_{\text{pump off}})$. Note the different y scale for $|b_{pp}|$.

field dependence, while the parameter $|a_{pp}|$ is approximately linear in field. These results appear consistent with expectation from depletion-EFISH. Any surface contribution that is not associated with the depletion electric field would be expected to yield a nonzero y-axis intercept for $|a_{pp}|$ in Fig. 4; the lack of a significant intercept suggests that any such term for oxidized GaAs surfaces is negligible. The lack of a significant intercept also supports the neglect of the quadrupolar parameter γ.

If the dominant source of a_{pp} is $\chi^{(3)} E_z^{(\text{depl})}$, then the sign of a_{pp} is determined by the sign of the depletion field. Figure 5 compares $S_{pp}(\phi)$ for n- and p-type samples. The change in sign of a is confirmed by the shift in the location of the maximum signal from along [110] on the n-type material to along [1̄10] for the p-type material. Unlike n-type material, where the surface Fermi level is pinned near midgap for almost all surface treatments, the pinning position on p-type material can vary widely. Using a surface potential of 0.17 eV taken from photoreflectance studies of P_2S_5-treated surfaces,[31] both $|a_{pp}|$ and $|b_{pp}|$ from the p-type sample are in good agreement with those observed on the n-type samples (see Fig. 4). It should be noted that it is important to make the comparison of dopants at the same probe photon energy. As can be seen from Fig. 3, $|\delta\phi_{ab}|$ changes from $<90°$ to $>90°$ as $h\nu$ is scanned from 1.3 to 1.17 eV, thus changing the sign of the interference between a and b and shifting the orientation of the maxima from along [110] at 1.3 eV to along [1̄10] at 1.17 eV.

Additional confirmation of the role of E_z^{depl} in second-harmonic generation from GaAs(001) can be obtained by photomodulation experiments.[32] Injection of a density of free carriers comparable to the background doping level will result in screening of the depletion field, and should modulate the depletion field contribution to SHG. Upon pumping with 2.33-eV light sufficient to generate $>10^{18}$ carriers/cm^3 (see Sec. V B), changes are observed in the rotational anisotropy. Figure 2 shows the 2.33-eV-pumped rotational distribution for the 3.8×10^{18}-cm^{-3} sample with a 1.38-eV probe. The trend is similar for all of the samples at all wavelengths: a very small increase in second harmonic intensity is observed for $S_{sp}(\phi)$, and a significant change toward fourfold symmetry is observed for $S_{pp}(\phi)$ and $S_{ps}(\phi)$. Photomodulated S_{pp} rotational patterns for all of the samples over the fundamental photon energy range of 1.32–1.51 eV were measured, and fitted to $|a_{pp}|$, $|b_{pp}|$, and $|\delta\phi_{ab}|$. In Fig. 6 is plotted the relative change, (pump on–pump off)/pump off, of $|a_{pp}|$ and $|b_{pp}|$ as a function of fundamental photon energy for all measured samples. The photomodulated data were taken by modulating the pump beam with a shutter at each point of a rotational scan. While the absolute values of the field parameters may be susceptible to systematic errors, their relative change with photomodulation is determined very precisely. No statistically significant modulation of $|b_{pp}|$ could be detected for the lightly doped samples at all probe energies. For the 3.8×10^{18} and 3.0×10^{18}-cm^{-3} n-type doped samples, $|b_{pp}|$ *increased* by approximately 5%. However, nearly all of the samples showed a *decrease* in $|a_{pp}|$ by approximately 50% over this wavelength range. These results are consistent with the dopant concentration studies. The dominant contribution to a_{pp} is from $\chi^{(3)}E_z^{(\text{depl})}$; therefore, a_{pp} exhibits sig-

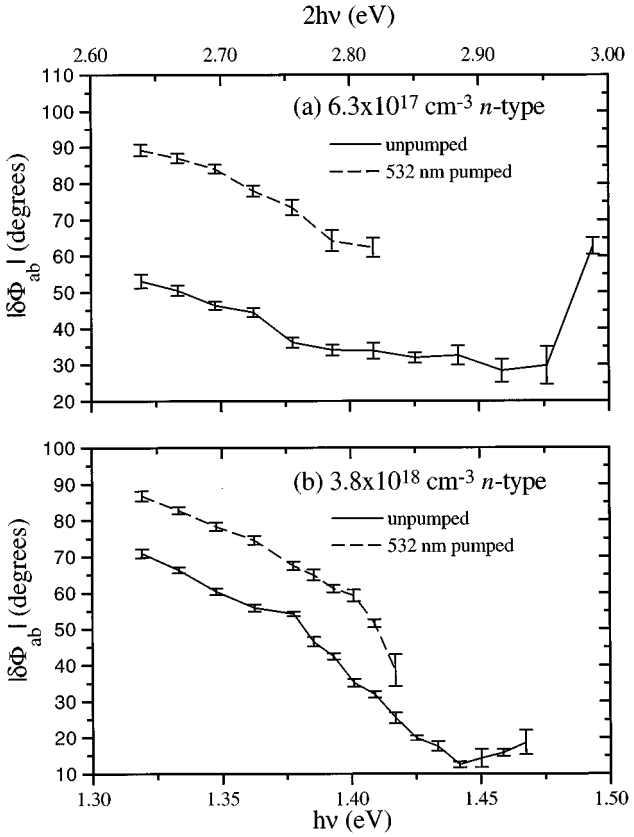

FIG. 7. The magnitude of the phase between a_{pp} and b_{pp}, with and without 532-nm pumping, as a function of wavelength for two of the n-type samples: (a) 6.3×10^{17} and (b) 3.8×10^{18} cm^{-3}. The indicated error bars are one standard deviation.

nificant photomodulation. In contrast, b_{pp} has very little contribution from $\chi^{(4)}E_z^{(\mathrm{depl})}E_z^{(\mathrm{depl})}$ and exhibits very little photomodulation.

Figure 7 displays $|\delta\phi_{ab}|$ with and without 532-nm pumping as a function of wavelength for the medium-doped and highly doped n-type samples. For fundamental energies greater than about 1.46 eV, $|a_{pp}|$ was too small upon pumping to extract a meaningful phase. Therefore, the results are not shown. Similarly, the measurements of $|\delta\phi_{ab}|$ for the lesser-doped samples did not exhibit a sufficient signal-to-noise-ratio to merit presentation, as $|a_{pp}|$ was again too small.

V. DISCUSSION

A. Data in the absence of photogenerated carriers

The phenomenological model developed in Sec. II parametrized the SHG response in terms of 11 complex numbers: $\chi^{(2)}_{xyz}$, $\chi^{(3)}_{zzzz}$, $\chi^{(3)}_{zxxz}$, $\chi^{(3)}_{xxzz}$, $\chi^{(4)}_{xyzzz}$, $\chi^{(4)}_{zxyzz}$, γ, ζ, Δ_{zzz}, Δ_{zxx}, and Δ_{xxz}. Based on the preceding discussion, ζ and γ will be neglected. The monotonic increase of $\langle a_{pp}\rangle$ with $E_z^{(\mathrm{depl})}$ indicates that $\chi^{(3)}$ terms must be included, while the small intercept at zero field indicates that the $\Delta^{(2)}$ terms can be neglected. Similarly, the observation that b_{pp} is independent of dopant concentration (for photon probe energies above 1.4 eV) and only weakly photomodulates at *all* studied probe photon energies indicates that $\chi^{(4)}$ is small. Neglecting $\chi^{(4)}$,

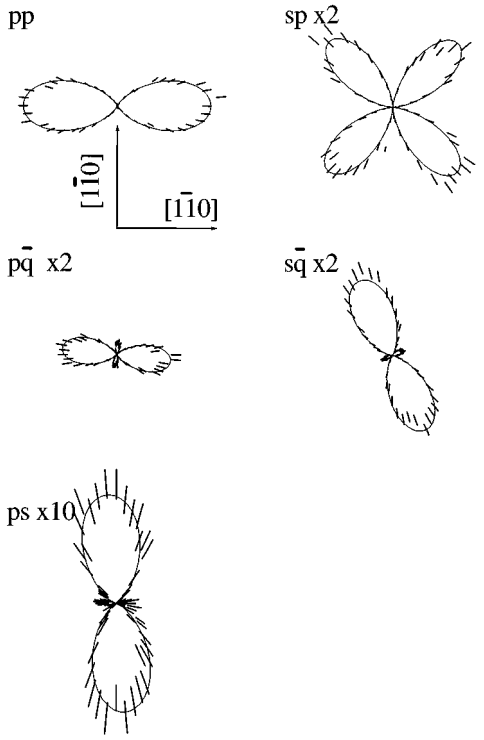

FIG. 8. SH signal as a function of azimuthal orientation for a 3.0×10^{18}-cm^{-3} n-type GaAs(001) sample at $\lambda_1=860$ nm for different input and detection polarizations. The solid lines are fits to the data as described in Sec. V A.

the SHG response can be characterized by only four complex numbers: $\chi^{(2)}_{xyz}$, $\chi^{(3)}_{zzzz}$, $\chi^{(3)}_{zxxz}$, and $\chi^{(3)}_{xxzz}$. From Eqs. (8), (10), and (12) we see that measurement of the three polarization combinations pp, ps, and $s\bar{q}$ allows extraction of the three complex ratios $\chi^{(3)}_{zzzz}/\chi^{(2)}_{xyz}$, $\chi^{(3)}_{zxxz}/\chi^{(2)}_{xyz}$, and $\chi^{(3)}_{xxzz}/\chi^{(2)}_{xyz}$. Shown in Fig. 8 are 860-nm SHG rotational anisotropy studies for the 3.0×10^{18}-cm^{-3} n-type sample for the polarization combinations: pp, $p\bar{q}$, ps, sp, and $s\bar{q}$. The complex field parameters a, b, and c can be explicitly expressed in terms of the susceptibility tensor elements weighted by complex numbers calculated from Eqs. (8)–(12) as follows:

$$a_{ij}=w_{a_{ij}}(zzzz)\chi^{(3)}_{zzzz}+w_{a_{ij}}(zxxz)\chi^{(3)}_{zxxz}+w_{a_{ij}}(xxzz)\chi^{(3)}_{xxzz},$$

$$b_{ij}=w_{b_{ij}}(xyz)\chi^{(2)}_{xyz}+w_{b_{ij}}(zxyzz)\chi^{(4)}_{zxyzz}+w_{b_{ij}}(xyzzz)\chi^{(4)}_{xyzzz}, \tag{28}$$

$$c_{ij}=w_{c_{ij}}(xyz)\chi^{(2)}_{xyz}+w_{c_{ij}}(zxyzz)\chi^{(4)}_{zxyzz}+w_{c_{ij}}(xyzzz)\chi^{(4)}_{xyzzz}.$$

The relevant weights for the data in Fig. 8 are given in Table II. The data for the pp, $p\bar{q}$, ps, and $s\bar{q}$ polarization combinations in Fig. 8 were fitted to Eq. (22). The 16 experimentally derived parameters: a_{pp}, b_{pp}, $|\delta\phi_{ab(pp)}|$, $a_{p\bar{q}}$, $b_{p\bar{q}}$, $c_{p\bar{q}}$, $|\delta\phi_{ab(p\bar{q})}|$, $|\delta\phi_{ac(p\bar{q})}|$, etc. were fit in a weighted least squares sense to six parameters: the real and imaginary parts of $\chi^{(3)}_{zzzz}/\chi^{(2)}_{xyz}$, $\chi^{(3)}_{zxxz}/\chi^{(2)}_{xyz}$, and $\chi^{(3)}_{xxzz}/\chi^{(2)}_{xyz}$ using the weights in Table II. Since the absolute phase of the second-harmonic field was not measured, the rotational anisotropy data only determine $|\delta\phi|$. Therefore the ps and $s\bar{q}$ data determine two possible values for the ratios $\chi^{(3)}_{zxxz}/\chi^{(2)}_{xyz}$, and $\chi^{(3)}_{xxzz}/\chi^{(2)}_{xyz}$. In

TABLE II. Computed weighting factors for the contribution of each susceptibility tensor to the measured field parameters. The fundamental wavelength was 860 nm, $E_z^{(\mathrm{depl})}(z=0)=8.18\times10^7$ V/m, and $L_d=16.6$ nm.

	$\chi^{(2)}_{xyz}$	$\chi^{(3)}_{zzzz}$ (V/m)	$\chi^{(3)}_{zxxz}$ (V/m)	$\chi^{(3)}_{xxzz}$ (V/m)
$w_{a_{pp}}$		$3.99\times10^3\ e^{i\ 1.62}$	$1.02\times10^5\ e^{i\ 1.64}$	$2.98\times10^5\ e^{-i\ 1.20}$
$w_{b_{pp}}$	$1.00\times10^{-3}\ e^{-i\ 0.302}$			
$w_{a_{p\bar{q}}}$		$2.00\times10^3\ e^{i\ 1.62}$	$8.74\times10^4\ e^{i\ 1.64}$	$1.49\times10^5\ e^{-i\ 1.20}$
$w_{b_{p\bar{q}}}$	$6.7\times10^{-4}\ e^{-i\ 0.420}$			
$w_{c_{p\bar{q}}}$	$2.5\times10^{-4}\ e^{i\ 0.071}$			
$w_{a_{ps}}$			$7.30\times10^4\ e^{i\ 1.64}$	
$w_{b_{ps}}$	$3.6\times10^{-4}\ e^{-i\ 0.756}$			
$w_{a_{s\bar{q}}}$				$1.01\times10^5\ e^{-i\ 1.23}$
$w_{b_{s\bar{q}}}$	$4.9\times10^{-4}\ e^{i\ 2.65}$			
$w_{c_{s\bar{q}}}$	$5.9\times10^{-4}\ e^{-i\ 0.487}$			
$w_{c_{sp}}$	$1.17\times10^{-3}\ e^{-i\ 0.487}$			

general, when combined with the pp data, there will be 2^3 possible values for $\chi^{(3)}_{zzzz}/\chi^{(2)}_{xyz}$. However, $|\delta\phi_{ab}|$ for the pp data is approximately 0, and thus there is no additional phase ambiguity and there are only four sets of susceptibility ratios. The four solutions for the ratios of the susceptibilities are given in Table III. The uncertainties are the estimated standard deviation based on the elements of the inverse of the curvature matrix.[23] Also listed in Table III, for each solution, is the total weighted variance per degree of freedom dof, $R=(1/\mathrm{dof})\sum_{t=1}^{npts}(1/\sigma_i^2)(S_i-M_i)^2$ where S_i are the experimental field parameters, σ_i are the estimated uncertainties of the field parameters, and M_i are the predicted field parameters from the model. The lines drawn in Fig. 8 are from solution set 1. The magnitudes of $\chi^{(3)}_{zxxz}$ and $\chi^{(3)}_{xxzz}$ are approximately equal, indicating that Kleinman symmetry (permutation of the indices independent of frequency) approximately holds. This suggests that solutions 1 and 2, which have similar phases for $\chi^{(3)}_{zxxz}$ and $\chi^{(3)}_{xxzz}$, are more likely correct. However, Kleinman symmetry is only strictly true in nonabsorbing materials.

The absolute magnitude of $\chi^{(2)}_{xyz}(-2\omega;\omega,\omega)$ has been measured by a number of researchers,[33–36] although all have neglected the possibility of depletion field effects. Significant discrepancies exist in both the magnitude and dispersion of the reported values for $\chi^{(2)}$; however, the reports suggest that $\chi^{(2)}$ is of the order of 4×10^{-10} m/V (1×10^{-6} esu). $\chi^{(3)}$ for third-harmonic generation (THG) of 1064 nm has been reported to be about 1×10^{-18} m^2/V^2 (1×10^{-10} esu).[37] Huang and Ching have calculated $\chi^{(2)}$ and $\chi^{(3)}$ for a large number of cubic semiconductors. For GaAs, they obtain[38]

$$\lim_{\omega\to0}\frac{\chi^{(3)}_{ijij}(-3\omega;\omega,\omega,\omega)}{\chi^{(2)}_{ijk}(-2\omega;\omega,\omega)}=2.3\times10^{-9}\ \text{m/V},$$

$$\lim_{\omega\to0}\frac{\chi^{(3)}_{iiii}(-3\omega;\omega,\omega,\omega)}{\chi^{(2)}_{ijk}(-2\omega;\omega,\omega)}=4.0\times10^{-9}\ \text{m/V}.$$

The measured $\chi^{(3)}_{zxxz}/\chi^{(2)}_{xyz}$ and $\chi^{(3)}_{xxzz}/\chi^{(2)}_{xyz}$ of $\approx3\times10^{-9}$ m/V (see Table III) are qualitatively consistent with the THG and SHG data and with the calculation. Note that due to the definition of the electric fields in Eq. (6), $\chi^{(3)}(-2\omega;\omega,\omega,0)$ as defined in Eq. (1), should be compared to $\chi^{(3)}(-3\omega;\omega,\omega,\omega)/2$ in Huang and Ching's calculations. However, the measured $\chi^{(3)}_{zzzz}/\chi^{(2)}_{xyz}$ of $\approx1\times10^{-7}$ m/V is an order of magnitude greater than expected from THG or theory. This may indicate that nonoptical contributions to $\chi^{(3)}(-2\omega;\omega,\omega,0)$, such as strain-induced terms from the converse piezoelectric effect, are important. Using the known value of the only nonzero piezoelectric tensor element[39] ($d_{xyz}=2.7\times10^{-10}$ cm/V) and the estimated $E_z^{(\mathrm{depl})}$, the maximum surface tensor shear stress ε_{xy} is 2.2×10^{-4}. Both theoretical[40] and experimental[41] studies of the sensitivity of SHG to stress suggest that $\varepsilon_{xy}=2.2\times10^{-4}$ is too small to account for the anomalous $\chi^{(3)}_{zzzz}$.

The dispersion of the field parameters shown in Fig. 3 reflects both the dispersion of ε_r, via $B^{(n)}_{s,p}$ and $f_{s,p}$ of Sec. II, and the dispersion of the nonlinear susceptibilities. In order to assess the influence of the dispersion of ε_r, a_{pp}, b_{pp}, and $|\delta\phi_{ab}|$ have been calculated from Eq. (8) as a function of dopant concentration assuming that $\chi^{(3)}_{zzzz}/\chi^{(2)}_{xyz}$, $\chi^{(3)}_{zxxz}/\chi^{(2)}_{xyz}$,

TABLE III. Susceptibility tensor ratios (in m/V) obtained by fitting field parameters from data in Fig. 8. The uncertainties are the estimated standard deviation of the fitting procedure (see text).

	soln 1	soln 2	soln 3	soln 4
$\chi^{(3)}_{zzzz}/\chi^{(2)}_{xyz}$	$9\pm1\times10^{-8}\times e^{i\ 2.64\pm0.11}$	$3.3\pm0.9\times10^{-8}\times e^{i\ 0.68\pm0.48}$	$1.6\pm0.2\times10^{-7}\times e^{-i\ 0.50\pm0.06}$	$2.4\pm0.1\times10^{-7}\times e^{i\ 2.41\pm0.04}$
$\chi^{(3)}_{zxxz}/\chi^{(2)}_{xyz}$	$3.4\pm0.1\times10^{-9}\times e^{i\ 1.26\pm0.05}$	$3.6\pm0.2\times10^{-9}\times e^{i\ 0.26\pm0.05}$	$3.4\pm0.1\times10^{-9}\times e^{i\ 1.26\pm0.05}$	$3.6\pm0.2\times10^{-9}\times e^{i\ 0.26\pm0.05}$
$\chi^{(3)}_{xxzz}/\chi^{(2)}_{xyz}$	$4.07\pm0.09\times10^{-9}\times e^{i\ 1.17\pm0.04}$	$4.06\pm0.08\times10^{-9}\times e^{i\ 0.32\pm0.04}$	$4.1\pm0.2\times10^{-9}\times e^{i\ 0.32\pm0.05}$	$4.06\pm0.08\times10^{-9}\times e^{i\ 1.17\pm0.04}$
R	1.46	1.74	1.46	1.74

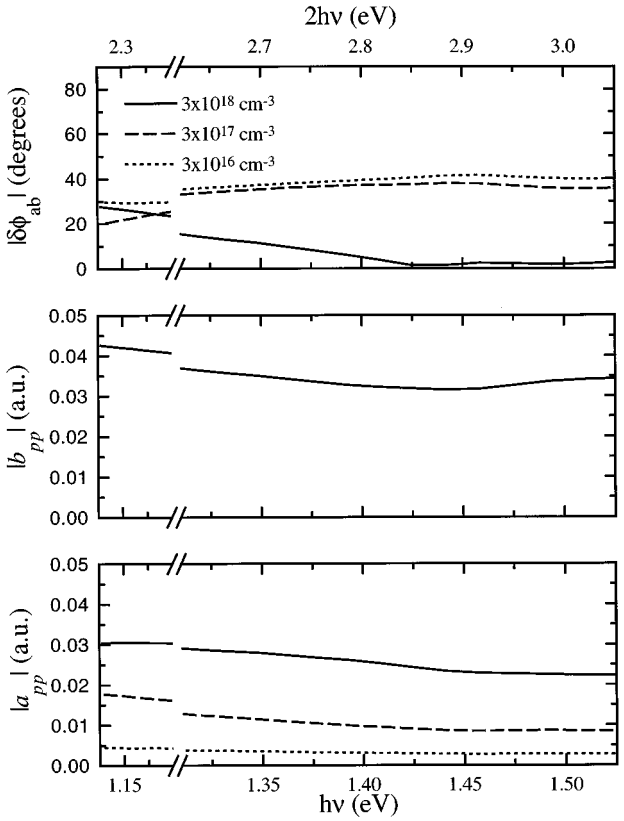

FIG. 9. The calculated amplitude and phases for the S_{pp} field parameters a, b, and $|\delta\phi|$ under the conditions that all orders of the nonlinear susceptibility are wavelength independent. The model was evaluated for three different n-type dopant concentrations: 3×10^{18} cm^{-3} (solid line), 3×10^{17} cm^{-3} (dashed line), and 3×10^{16} cm^{-3} (dotted-dashed line).

and $\chi^{(3)}_{xxzz}/\chi^{(2)}_{xyz}$ are as given in Table III, solution 1, and that all nonlinear χ's are dispersionless and independent of doping (see Fig. 9). The spectral behavior of each of the calculated field parameters is relatively flat over the wavelength range of interest. The dispersion in ε_r produces a weak structure near the one-photon resonance at E_0 ($\hbar\omega$=1.42 eV) and the two-photon resonance at $E_1(\hbar 2\omega$=2.98 eV). These calculations do not include changes in ε_r that result from changes in the dopant concentration or the presence of free carriers; such changes are expected to yield only small modifications to the results shown in Fig. 9. Comparison of the data in Fig. 3 with the calculations in Fig. 9 indicate that the prominent features in the *data*: a dispersive feature in $|\delta\phi_{ab}|$ near 1.45 eV and the monotonic increase in b for energies below 1.40 eV on the 5×10^{16}-cm^{-3} and semi-insulating samples are not due to dispersion in ε_r, and are attributed to dispersion in the nonlinear χ's.

Based on Fig. 9, one expects to see two trends in the data as a function of dopant concentration if a_{pp} is dominated by $\chi^{(3)}E_z^{(\mathrm{depl})}$: a monotonic increase in $|a_{pp}|$ with increasing doping, and a monotonic shift in $|\delta\phi_{ab}|$. In general, $|a_{pp}|$ does not vary simply with the depletion field; it is determined by a complex function of $E_z^{(\mathrm{depl})}(z=0)$, L_D, and ω (through the phase factor p). Since both $E_z^{(\mathrm{depl})}(z=0)$ and L_D vary with dopant concentration, care must be taken in interpreting the linear trend in Fig. 4. However, from Fig. 9, it is clear that over the range of dopant concentrations and photon energies studied in this work, a linear relationship does exist between $|a_{pp}|$ and $E_z^{(\mathrm{depl})}$, and the interpretation of Fig. 4 as support for a dominant $\chi^{(3)}$ contribution to a_{pp} is valid.

While the trend in $|a_{pp}|$ is quantitatively understood in terms of the model of Sec. II, and the assumption that a_{pp} is dominated by $\chi^{(3)}E_z^{(\mathrm{depl})}$, the behavior of $|\delta\phi_{ab}|$ is puzzling. The dispersive 2ω feature in $|\delta\phi_{ab}|$ at 1.45 eV is probably related to the high joint density of states that gives rise to the E_1 absorption at 2.98 eV. If the relative phase angle between $\chi^{(3)}$ and $\chi^{(2)}$ was independent of dopant concentration, then one would expect $|\delta\phi_{ab}(\omega)|$ to exhibit trends similar to those in Fig. 9, i.e., exhibit approximately parallel positive shifts with increasing dopant concentration. From Fig. 3 it is clear that this does not occur; $|\delta\phi_{ab}|$ for the 6.2×10^{17}-cm^{-3} doped sample crosses that for the two nominal 3×10^{18}-cm^{-3} doped samples. This implies that the relative phase angle between $\chi^{(2)}$ and $\chi^{(3)}$ must vary with dopant concentration. From linear optical studies,[42] it is clear that the electronic structure of GaAs varies with doping, due to both Burstein-Moss shifts and impurity potential scattering. The implications of such phenomena on the nonlinear properties have not been extensively characterized.

A Kramers-Kronig relationship exists between the real and imaginary parts of $\chi^{(2)}(-2\omega;\omega,\omega)$;[43] therefore, the dispersive feature in $|\delta\phi_{ab}|$ near 1.45 eV would be expected to be associated with a dispersive feature in the magnitude of either a_{pp} or b_{pp}. The data in Fig. 3 do not suggest any strong features in b_{pp} at 1.45 eV; however, a weak suggestion of a peak is observed in a_{pp} for the 3.8×10^{18}-cm^{-3} doped sample. This peak would be more prominent if the dispersion of the linear weighting factors (see Fig. 9) were taken into account.

The strong increase in $|b_{pp}|$ for the 5×10^{16}-cm^{-3} and semi-insulating samples at photon energies below the fundamental gap is intriguing. As no statistically significant photomodulation of this signal could be detected, the increase cannot be associated with the weak depletion field of the low-doped samples. A similar dispersion in SHG mixing has been reported by Zhang *et al.*[44] on semi-insulating GaAs(111) samples. The low carrier densities in semi-insulating material are generally attributed to the presence of deep traps due to the EL2 defect, which can be characterized by its strong optical absorption near 1.2 eV.[45] It is possible that the strong signal below the fundamental gap could be associated with an EL2-like defect. Studies characterizing the effect of EL2 density on the SHG response are merited.

B. Data in the presence of photogenerated carriers

Photomodulation of the optical response of semiconductor materials has proven to be a powerful technique, perhaps best represented by photoreflectance spectroscopy.[46] In the current work, photomodulation studies were conducted to validate the interpretation of the rotational anisotropy studies in terms of dominant $\chi^{(2)}$ and $\chi^{(3)}$ contributions, and to clarify any $\chi^{(4)}$ contributions. Qualitatively, the photomodulation studies are in excellent agreement with the interpretation of the doping-dependent rotational anisotropy studies. In this section, we explore the quantitative implications of the

photomodulation results, most notably that the 532-nm pump light causes only a ≈50% decrease in $|a_{pp}|$ for all probe photon energies and dopant concentrations. In addition to screening $E_z^{(\mathrm{depl})}$, the free carriers generated by the 532-nm pump light will alter the linear dielectric response of the system via the introduction of free-carrier absorption, and can introduce contributions to the nonlinear response. At the relatively low levels of injection used (see the following discussion), the small changes in the linear dielectric response will be neglected. Similarly, we will neglect any changes in the χ's due to the free carriers.

The proper calculation of the time-dependent carrier profiles at injection levels comparable to the background dopant concentration is a complicated and daunting task. Assuming a drift-diffusion model will be appropriate to the long (ps) time-scale response characteristic of the measurements, one still must self-consistently treat the injected electrons, holes, and space-charge field with proper surface recombination boundary conditions. If the population of fast traps make a significant contribution to the surface charge boundary condition, the calculation becomes extremely difficult.[47] Nonetheless, with some simplification, insight into the behavior can be gained. A good approximation to the analytic solution to the injected surface carrier density n_{inj} at the end of a square pulse of duration t_p, for flatband conditions with surface recombination, is

$$n_{\mathrm{inj}}(z=0)=\frac{(1-R)F}{\alpha^{-1}+\sqrt{D\tau_R}}\left[\frac{1}{1+S\tau_R/\sqrt{D\tau_R}}\right], \qquad (29)$$

where R is the reflectivity, F is the total pulse fluence (photons/cm^2), D the ambipolar diffusion constant (cm^2/s), and S the surface recombination velocity (cm/s). τ_R is a reduced time, the root reciprocal square average of the pulse duration and the bulk recombination lifetime.[48] For our 532-nm pump pulse ($F\approx 1\times10^{15}$ photons/cm^2), the estimated surface carrier density[49] lies in the range 2×10^{18}–2×10^{19} cm^{-3} for $0\leqslant S\leqslant 10^6$ cm/s. Since the estimate of the injected carrier density is comparable to or exceeds the doping level of all samples, it is likely that the 532-nm pulse completely ''flattens'' the bands, i.e., the surface potential is not expected to differ from the bulk potential by more than a few kT.

If one assumes that the fixed charge ($N_s=-2.4\times10^{12}$ e/cm^2 for $N=6.2\times10^{17}$ cm^{-3}) at the interface responsible for the 0.68 eV of band bending in the dark is not changed by photoinjection (i.e., all the charges are slow traps in the oxide), then the electric field at $z=0$ is not altered by photoinjection. This field is screened by the essentially neutral, photoinjected plasma. This is similar to the problem of calculating the depletion field in an intrinsic semiconductor. Following the discussion of Ref. 50, it can be shown that a good approximation to the electric field for large n_{inj} is

$$E(z)=\exp\left(\frac{-z}{L_{\mathrm{inj}}}\right),$$

where (30)

$$L_{\mathrm{inj}}^2=\frac{kT\varepsilon_r\varepsilon_0}{2q^2n_{\mathrm{inj}}},$$

k is Boltzmann's constant, T is the sample temperature, and L_{inj} is a screening length. For $n_{\mathrm{inj}}=(1\text{ to }10)\times10^{18}$ cm^{-3} and $L_{\mathrm{inj}}=10$–3.2 nm.

Naively, one would think that this very strongly screened field (contrast $L_{\mathrm{inj}}\approx5$ nm, with $L_D\approx100$ nm due to the depletion field screening) would result in significantly less contribution to the SHG from $\chi^{(3)}E_z^{(\mathrm{depl})}$, in apparent contrast to the observed uniform depletion of only 50%. However, a quantitative application of the model of Sec. II indicates that the SHG measurement is very sensitive to the magnitude of the screened electric field *at the surface*. This is because the phase factor pz oscillates with a very high spatial frequency. To compare the SHG signal from a sample in the dark with a ''flattened'' sample, we need to compare the following integrals:

$$\mathrm{dark}\propto E_0\int_{-L_d}^{0}\left(1+\frac{z}{L_d}\right)e^{-ipz}dz$$

and (31)

$$\mathrm{flat}\propto E_0\int_{-\infty}^{0}e^{-z/L_{\mathrm{inj}}}e^{-ipz}dz,$$

since the complex quantity $(a_{\text{pump on}}-a_{\text{pump off}})/a_{\text{pump off}}$ = (flat-dark)/dark.

For physically realistic values of $L_{\mathrm{inj}}(\approx5$ nm), the residual field in the flatband condition can produce contributions to the SHG of order $\frac{1}{2}$ those of the dark system. As the model assumes the surface field is fixed by the slow charges, $(a_{\text{pump on}}-a_{\text{pump off}})/a_{\text{pump off}}$ will be independent of doping, so long as the *dark* integral is independent of L_D. Since the observed $|a_{pp}|$ terms are linear in E, we are clearly in a domain where *dark* is independent of L_D. Thus the observation of only partial modulation of $|a_{pp}|$, and the dopant concentration independence of the modulation of a_{pp}, are consistent with completely flattened surface potentials and photoinjection-independent surface boundary charges. As the samples were oxidized, it is not surprising that a significant number of slow traps are present.

The preceding model also predicts a phase change for a_{pp} between pumped and dark measurements of order 40° to 50°. This is in qualitative agreement with the results in Fig. 7. The above discussion assumes that the sample is nondegenerate; however, $N_D=1\times10^{18}$ cm^{-3} is about the threshold for degenerate behavior. This is not anticipated to significantly affect the qualitative results.

Within the approximations that $|a_{pp}|$ is entirely due to $\chi^{(3)}$ contributions, and that the space-charge fields can be given by Eq. (17) in the dark, and Eq. (30) when optically pumped, one can use the observed 0.4–0.6 decrease in $|a_{pp}|$ when pumped to determine L_{inj} to be 3–5 nm. Using 4 nm to calculate the parameter $B_s^{(4)}$ [see Eq. (16)], we can estimate the ratio $\chi^{(4)}_{zxyzz}/\chi^{(2)}_{xyz}$ from the photomodulation of the sp data in Fig. 2. The ratio of the field parameter $c_{sp}^{\text{pump on}}/c_{sp}^{\text{pump off}}$ obtained by fitting the data in Fig. 2 to Eq. (22) is 1.036 ± 0.004. From this, we estimate $|\chi^{(4)}_{zxyzz}/\chi^{(2)}_{xyz}|$ to be in the range 2–8×10^{-18} m^2/V^2. The width of the range is dominated by the ambiguity in the relative phase between $\chi^{(4)}$ and $\chi^{(2)}$, and not the measurement uncertainty. Similarly, the photomodulation of the ps data in Fig. 2

($b_{ps}^{\text{pump on}}/b_{ps}^{\text{pump off}}=1.02\pm0.02$) establishes $|\chi^{(4)}_{xyzzz}/\chi^{(2)}_{xyz}|$ to be in the range $0–8\times10^{-18}$ m^2/V^2. The authors are not aware of any measurements of $\chi^{(4)}$ for GaAs. For a simple, cubicly anharmonic oscillator, the ratio $\chi^{(4)}/\chi^{(2)}$ is of the order of $\chi^{(3)}$, qualitatively consistent with our results ($\chi^{(3)}\approx10^{-18}$ m^2/V^2). However, the same simple model predicts $\chi^{(3)}/\chi^{(2)}$ to be of the order of $\chi^{(2)}$, and underestimates $\chi^{(3)}$ ($\chi^{(2)}\approx4\times10^{-10}$ m/V, while $\chi^{(3)}/\chi^{(2)}\approx3\times10^{-9}$ m/V).

C. Relationship to previous work

The principal observation in this study is that the EFISH contribution to the nonlinear response is larger than that from the oxide surface for dopant concentrations $\geqslant10^{16}$ cm^{-3}, and is of comparable magnitude to the bulk response at higher dopant concentrations. This is consistent with a recent SHG study of Au/GaAs Schottky barriers as a function of junction bias and SHG probe intensity.[15,16] Additionally, our results support the proposal of Yamada, Kimura, and Fuqua that a correlation observed between ''surface-sensitive'' SHG and simultaneously obtained photoluminescence during photowashing of GaAs wafers was due to unpinning of the Fermi level combined with an EFISH contribution to the SHG.[51] It should be noted that the SHG probe in Ref. 51 was a 560-nm pulsed dye laser at incident fluences sufficient to flatten the bands due to photoinjection of carriers completely. Therefore the SHG is probing the residual field after screening of the slow interface states by the photoinjected carriers.

When considering the possible role of EFISH contributions to surface nonlinear optical experiments, it is extremely important to account for probe-induced photovoltage effects, especially when comparing probe wavelengths with significantly different substrate absorption coefficients. For example, in an early study of the rotational anisotropy from oxide-covered, highly-doped GaAs by Hollering,[11] an increase in $|a_{pp}|$ (attributed entirely to $\Delta^{(2)}$ terms) relative to $|b_{pp}|$ for SHG at 1.16-eV probe energies compared to 2.33-eV probe energies was interpreted in terms of a resonance enhancement of a_{pp} at 1.16 eV. We see no evidence for such a resonance in a_{pp}, although in lower doped samples we see enhancement in b_{pp}. The anisotropy of our data agrees well with that of Hollering at 1.16 eV. It is possible that the decrease in a_{pp} observed at 2.33 eV by Hollering was due, at least in part, to probe-induced screening of the surface depletion field, and the a_{pp} contribution reported by Hollering arises from $\chi^{(3)}E_z^{(\text{depl})}$. The 532-nm probe laser in Hollering's study was of comparable duration and fluence to the 532-nm photomodulation source in our study.

The conclusions of this paper, that $\chi^{(3)}E_z^{\text{depl}}$ contributes significantly to the observed SHG, and that $\chi^{(4)}(E_z^{\text{depl}})^2$ is small, are in contradiction to a recent report by Qi *et al.*,[12] where $\chi^{(3)}$ effects were not observed, but a significant variation of $\chi^{(\text{eff})}$ with both dopant concentration and photomodulation was observed and attributed to $\chi^{(4)}$. Significant differences exist in the work of Ref. 12 and this paper: they characterized samples of dopant concentrations $\leqslant10^{16}$ cm^{-3}, used a ns pulse duration dye laser for the probe light, and used a relatively weak (100 μW/cm^2) 456-nm cw source for photomodulation. For our lightly doped samples, a_{pp} is very small relative to b_{pp}, and it is difficult to characterize the photomodulation of a_{pp}; however, the absence of significant photomodulation of b_{pp} is quite apparent (see Fig. 6). Realistic estimates of the near surface photoinjected carrier densities for the cw source used in Ref. 12, self-consistently accounting for surface recombination and drift in the space-charge region,[52] indicate that the steady-state density of injected carriers is only 10^{10} cm^{-3}. This is significantly less than the doping level, and suggests no significant modulation of the surface depletion field was achieved. Qi *et al.* observed[53] that photomodulation of b_{pp} was only detectable for a narrow range of probe photon energies around 1.34 eV, near the anomalous dispersion in b_{pp} observed in our work, and that of Refs. 44 and 33. As noted earlier, the EL2 defect plays a significant role in determining the electrical properties of semi-insulating and low carrier density GaAs. The EL2 defect has a characteristic optical absorption in the 1.1–1.3-eV range, resulting in the formation of a metastable excited state. Considering the high fluence of the 1.34-eV SHG *probe* laser in the work of Qi *et al.*, it is possible that their reported photomodulation is the result of changes in a probe-induced metastable EL2-like state.

VI. CONCLUSION

By careful study of the doping and photomodulation dependence of the SHG rotational anisotropy on oxidized GaAs(001), we established that the dominant contribution to the isotropic response from the near-surface region arises from a depletion-electric-field-induced effect, and that true surface contributions are small. The magnitude of the phenomenological expansion coefficients $\chi^{(3)}_{zxxz}(-2\omega;\omega,\omega,0)$, $\chi^{(3)}_{xxzz}(-2\omega;\omega,\omega,0)$, $\chi^{(4)}_{xyzzz}(-2\omega;\omega,\omega,0,0)$, and $\chi^{(4)}_{zxyzz}(-2\omega;\omega,\omega,0,0)$ are in accord with expectations based on theory and previous measurements. The coefficient $\chi^{(3)}_{zzzz}(-2\omega;\omega,\omega,0)$ is larger than anticipated. As stated in Sec. I, EFISH contributions to SHG have been identified in electrochemical studies of Si (Ref. 13) and TiO_2.[14] In both systems, the EFISH contribution could be made to dominate the depletion-field-independent contributions (surface and bulk). EFISH contributions thus appear to be general, implying that extreme care must be used in the interpretation of SHG results when either probe or photomodulation sources are outside the region of transparency of the sample. If the dynamical evolution of depletion-field-independent terms can be neglected, EFISH should prove a powerful probe of carrier dynamics via photovoltage effects.[14,54]

ACKNOWLEDGMENTS

L.J.R. wishes to acknowledge extensive discussions with J. Dagata on GaAs surface treatments, O. Glembocki on surface Fermi-level positions, and A. Yodh and J. Qi on their work.

APPENDIX

In this appendix, we review the various Fresnel coefficients. Given an incident angle θ with respect to the surface normal, and angular frequency ω,

$$f_s=\frac{n_0}{n}\sin\theta \tag{A1}$$

and

$$f_c = \sqrt{1 - f_s^2}, \tag{A2}$$

where n_0 and n are the complex index of the incident media and the substrate at the fundamental wavelength. The transmission coefficients for s- and p-polarized light are given by

$$t_s = \frac{2w_0}{w_0 + w} \tag{A3}$$

and

$$t_p = \frac{2n_0 n w_0}{w_0 n^2 + w n_0^2}, \tag{A4}$$

where

$$w = \frac{\omega}{c}\sqrt{n^2 - n_0^2 \sin^2\theta} \tag{A5}$$

and

$$w_0 = \frac{\omega n_0}{c}\sqrt{1 - \sin^2\theta}. \tag{A6}$$

Expressions for F_s, F_c, T_s, T_p, W, and W_0 are readily derived from the above with the replacements $\omega \rightarrow 2\omega$, $n \rightarrow N$, and $n_0 \rightarrow N_0$. In the expressions for T_s and T_p, the indices are reversed, i.e., $w_0 \rightarrow W$, $w \rightarrow W_0$, etc., as the T's are the transmission factors for the *exiting* second harmonic.

*Permanent address: School of Chemistry, The University of Birmingham, Edgbaston, Birmingham B15 2TT, United Kingdom.
†Electronic address: lee.richter@nist.gov

[1] Y. R. Shen, Ann. Rev. Phys. Chem. **40**, 327 (1989); Surf. Sci. **299/300**, 551 (1994).
[2] R. M. Corn and D. A. Higgins, Chem. Rev. **94**, 107 (1994).
[3] P. Guyot-Sionnest and Y. R. Shen, Phys. Rev. B **38**, 7985 (1988).
[4] T. Stehlin, M. Feller, P. Guyot-Sionnest, and Y. R. Shen, Opt. Lett. **13**, 389 (1988).
[5] C. Yamada and T. Kimura, Phys. Rev. B **49**, 14 372 (1994).
[6] C. Yamada and T. Kimura, Phys. Rev. Lett. **70**, 2344 (1993).
[7] D. S. Buhaenko, S. M. Francis, P. A. Goulding, and M. E. Pemble, J. Cryst. Growth **97**, 591 (1989).
[8] S. R. Armstrong, R. D. Hoare, M. E. Pemble, I. M. Povey, A. Stafford, and A. G. Taylor, J. Cryst. Growth **120**, 94 (1992); C. Yamada and T. Kimura, *ibid.* **130**, 321 (1993); S. R. Armstrong, R. D. Hoare, M. E. Pemble, I. M. Povey, A. Stafford, and A. G. Taylor, *ibid.* **130**, 323 (1993).
[9] S. R. Armstrong, R. D. Hoare, M. E. Pemble, I. M. Povey, A. Stafford, A. G. Taylor, B. A. Joyce, J. H. Neave, and J. Zhang, Surf. Sci. **291**, L751 (1993).
[10] M. E. Pemble, A. Stafford, and A. G. Taylor, Appl. Surf. Sci. **54**, 490 (1992).
[11] R. W. J. Hollering, Opt. Commun. **90**, 147 (1992).
[12] J. Qi, M. S. Yeganeh, I. Koltover, A. G. Yodh, and W. M. Theis, Phys. Rev. Lett. **71**, 633 (1993).
[13] P. R. Fischer, J. L. Daschbach, and G. L. Richmond, Chem. Phys. Lett. **218**, 200 (1994); P. R. Fischer, J. L. Daschbach, D. E. Gragson, and G. L. Richmond, J. Vac. Sci. Technol. A **12**, 2617 (1994).
[14] J. M. Lantz, R. Baba, and R. M. Corn, J. Phys. Chem. **97**, 7392 (1993); J. M. Lantz and R. M. Corn, J. Phys. Chem. **98**, 9387 (1994).
[15] T. Rasing, Appl. Phys. A **59**, 531 (1994).
[16] W. de Jong, A. F. van Etteger, C. A. van't Hof, P. J. van Hall, and Th. Rasing, Surf. Sci. **331**, 1372 (1995).
[17] The usual coordinate system for $mm2$ has mirror operations $(x,y,z) \rightarrow (-x,y,z)$ and $(x,y,z) \rightarrow (x,-y,z)$. Here we rotate the coordinate system by 45°, so that the mirror operations are $(x,y,z) \rightarrow (y,x,z)$ and $(x,y,z) \rightarrow (-y,-x,z)$. These mirror operations are also elements of the $43m$ symmetry group.
[18] J. E. Sipe, D. J. Moss, and H. M. van Driel, Phys. Rev. B **35**, 1129 (1987).
[19] J. E. Sipe, J. Opt. Soc. Am. B **4**, 481 (1987).
[20] C. M. Wolf, N. Holonyak, Jr., and G. E. Stillman, *Physical Properties of Semiconductors* (Prentice-Hall, Englewood Cliffs, N.J., 1989), p. 317.
[21] J. Rudnick and E. A. Stern, Phys. Rev. B **4**, 4274 (1971).
[22] From Poisson statistics, the probability $P(x,\mu)$ of having x counts when the expected value is μ is given by $\mu^x e^{-\mu}/x!$. Summing over all $x \geq 1$, the probability of one or more photons reaching the detector is $1-e^{-\mu}$. Thus $\mu = -\ln(1-\langle x \rangle)$.
[23] P. R. Bevington, *Data Reduction and Error Analysis for the Physical Sciences* (McGraw-Hill, New York, 1969), p. 242.
[24] K. Kato, IEEE J. Quantum Electron. **22**, 1013 (1986).
[25] R. C. Eckardt, H. Masuda, Y. X. Fan, and R. L. Byer, IEEE J. Quantum Electron. **26**, 922 (1990).
[26] J. A. Dagata, W. Tseng, J. Bennett, J. Schneir, and H. H. Harary, Ultramicroscopy **42–44**, 1288 (1992).
[27] E. A. Caridi and T. Y. Chang, J. Electrochem. Soc. **131**, 1440 (1984).
[28] D. J. Bottomley, G. Lüpke, J. G. Mihaychuk, and H. M. van Driel, J. Appl. Phys. **74**, 6072 (1993). Note that if the crystal is miscut, such that the depletion field is not strictly along the $\hat{\mathbf{z}}$ direction, the results of Bottomley *et al.* will be modified to a small degree.
[29] J. E. Sipe, V. Mizrahi, and G. I. Stegeman, Phys. Rev. B **35**, 9091 (1987).
[30] G. Lüpke, D. J. Bottomley, and H. M. van Driel, J. Opt. Soc. Am. B **11**, 33 (1994).
[31] O. J. Glembocki, J. A. Tuchman, K. K. Ko, S. W. Pang, J. A. Dagata, A. Giordana, R. Kaplan, and C. E. Stutz, Proc. SPIE **2141**, 96 (1994); O. J. Glembocki, J. A. Tuchman, K. K. Ko, S. W. Pang, A. Giordana, R. Kaplan, and C. E. Stutz, Appl. Phys. Lett. **66**, 3054 (1995).
[32] M. S. Yeganeh, J. Qi, A. G. Yodh, and M. C. Tamargo, Phys. Rev. Lett. **68**, 3761 (1992).
[33] F. G. Parsons and R. K. Chang, Opt. Commun. **3**, 173 (1971).
[34] H. Lotem, G. Koren, and Y. Yacoby, Phys. Rev. B **9**, 3532 (1974).
[35] R. K. Chang, J. Ducuing, and N. Bloembergen, Phys. Rev. Lett. **15**, 415 (1965).
[36] M. S. Yeganeh, J. Qi, J. P. Culver, A. G. Yodh, and M. C. Tamargo, Phys. Rev. B **46**, 1603 (1992).
[37] W. K. Burns and N. Bloembergen, Phys. Rev. B **4**, 3437 (1971).
[38] M.-Z. Huang and W. Y. Ching, Phys. Rev. B **47**, 9479 (1993).
[39] G. Arlt and P. Quadflieg, Phys. Status Solidi **25**, 323 (1968).
[40] Z. H. Levine and D. C. Allan, Phys. Rev. B **44**, 12 781 (1991).
[41] G. D. Boyd, F. R. Nash, and D. F. Nelson, Phys. Rev. Lett. **24**, 1298 (1970).

[42] F. Lukeš, S. Gopalan, and M. Cardona, Phys. Rev. B **47**, 7071 (1993).
[43] S. Scandolo and F. Bassani, Phys. Rev. B **51**, 6925 (1995).
[44] X.-C. Zhang, Y. J. K. Ware, X. F. Ma, A. Rice, D. Bliss, J. Larkin, and M. Alexander, Appl. Phys. Lett. **64**, 622 (1994).
[45] G. M. Martin, Appl. Phys. Lett. **39**, 747 (1981).
[46] O. J. Glembocki, Proc. SPIE **1286**, 1 (1990), and references therein.
[47] N. J. Halas and J. Bokor, Phys. Rev. Lett. **62**, 1679 (1989).
[48] L. J. Richter and R. R. Cavanagh, Prog. Surf. Sci. **39**, 155 (1992).
[49] The parameters used in the calculation were $R_s=0.472$, $\alpha=8.3\times10^4$ cm^{-1}, $\tau_R=179$ ps, and $D=5.0$ cm^2/s.
[50] C. M. Wolf, N. Holonyak, Jr., and G. E. Stillman, *Physical Properties of Semiconductors* (Ref. 20), pp. 281 and 282.
[51] C. Yamada, T. Kimura, and P. Fuqua, Jpn. J. Appl. Phys. **31**, L1657 (1992).
[52] PC-1d ver. 3, Sandia Report No. SAND91-0516, 1991 (unpublished). Reference to this program is included for completeness of exposition, and constitutes neither an endorsement by the U.S. National Institute of Standards and Technology nor representation that the product so referenced is the best available for the purpose.
[53] J. Qi (personal communication).
[54] W. de Jong, A. F. van Etteger, C. A. van't Hof, P. J. van Hall, and Th. Rasing, Surf. Sci. **352**, 807 (1996).